SCIENTIFIC REPORTS

OPEN

SUBJECT AREAS:
POLYMERIZATION MECHANISMS
POLYMER CHARACTERIZATION
ELECTRONIC DEVICES
POLYMER SYNTHESIS

Received
18 April 2013

Accepted
25 July 2013

Published
12 August 2013

Correspondence and requests for materials should be addressed to M.Y. (yoshimur@mail.ncku.edu.tw)

Submerged Liquid Plasma for the Synthesis of Unconventional Nitrogen Polymers

Jaganathan Senthilnathan, Chih-Chiang Weng, Jiunn-Der Liao & Masahiro Yoshimura

Promotion Centre for Global Materials Research (PCGMR), Department of Material Science and Engineering, National Cheng Kung University, Tainan, Taiwan.

Glow discharge polymerization is not well understood due to the rapid/complex reaction at the plasma/gas precursor interface. Plasma reaction in a submerged condition allows post-plasma-polymerization, leading to further polymer growth and thus a stable structure. Electron collision with acetonitrile at the interface initiates the formation of radical monomers, which undergoes further rearrangement to form low-molecular (LM) nitrogen polymers (NPs). The radical-rich LM NPs go through further polymerization, forming stable high-molecular (HM) NPs (as determined using liquid chromatography/mass spectrometry). LM NPs absorb light at a wavelength of 270 nm (λ max) whereas HM NPs show absorption at 420 nm (λ max), as determined from ultraviolet-visible absorption spectra. The fluorescence spectra of HM NPs show characteristic emission at 430 nm, which indicates the presence of nitrogen functional groups with external conjugation. The proposed structure of HM NPs is verified with different analytical instruments.

Plasma processes are important for the synthesis of various types of materials[1,2]. Glow discharge plasma is a well-known technique for the polymerization of various organic compounds, including naphthalene, ethylene, perfluorocarbons, acetonitrile, acrylonitrile, pyridine, ferrocene, 1,2-dicyanoethylene, and tetracyanoethylene[3–6]. The polymerization of organic compounds using the glow discharge technique is however not fully understood due to the complex roles played by the organic compounds and their functional groups[6,7]. Glow discharge polymerization with a gaseous precursor has major shortcomings, including (a) high operation cost, (b) process complexity, (c) low contact time, which prevents complete carbonization or polymerization, (d) material loss, (e) and uncertainty and inconsistency in the end product. The present study thus proposes a submerged liquid plasma process. Plasma reaction in a submerged condition is an attractive tool for the formation of polymeric materials. The submerged liquid plasma reaction gives information about the reaction pathway and intermediates formed during the polymerization. The direct carbonization/polymerization of organic compounds in a submerged plasma condition is a soft solution process at ambient conditions[8–10]. The formation of plasma in aqueous solutions facilitates metal oxide powder synthesis[11,12], the formation of nanomaterials[13,14], the removal of organic pollutants from wastewater[15], hydrogen production[16], disinfection[17], reduction of metal ion[18], medical applications[19], and analytical tools[20]. In a plasma reaction, the organic solvent undergoes a carbonization or polymerization reaction depending on its functional groups. At the interface of plasma and the organic solvent, polymerization is induced by radicals rather than ions[6]. Under a plasma condition, methanol[21], ethanol[10,22,23], and other saturated aliphatic organic compounds form less stable radical species and polymerization is not favorable. In contrast, organic compounds with either unsaturated or high-energy functional groups (e.g., C=C, C=N, and C≡N) form stable free-radical monomers and initiate the polymerization reaction[24,25]. The formation of a plasma polymer in a submerged condition depends on the nature of the plasma formed, the chemical structure of the precursor, and the precursor functional group[26]. The chemical properties of polymers produced in plasma differ greatly from those of conventional polymers. The most significant differences are that the polymers produced by a plasma process do not contain regular or repeating units and are enriched with radicalized functional groups[27]. Plasma polymers offer a number of advantages over conventional polymers. Plasma-activated polytetrafluoroethylene significantly enhances the adhesion properties of steel[28]. Compounds polymerized under plasma have a higher dielectric property due to the existence of polar groups and that can be used for various electrical applications[6,28]. Plasma polymers are a potential replacement for conductive/functionalized polymers currently used as electrode materials, storage devices, light harvesting, solar

cells, gas storage, DNA probing, sensors, polymer-based batteries, light-emitting diodes, and super capacitors[29–34]. Conductive and fluorescent polymers can be synthesized only via the polymerization of fluorescent monomers or the modification of a commercially available polymer by adding/replacing reactive groups[35]. In the present study, a submerged liquid plasma technique is adopted for the direct (one-step) synthesis of nitrogen polymers (NPs). Acetonitrile is used as the target material for the formation of NPs. The NPs are characterized and the reaction mechanism and possible applications are evaluated.

Results

Formation of LM and HM NPs in submerged liquid plasma. At the start of the experiment, the tungsten-needle-to-Si-electrode distance was adjusted to get the maximum plasma width (Fig. 1a). When the tungsten needle touched the silicon electrode, there was no plasma observed in the solution. Plasma torch widths of 77, 141, and 213 μm were obtained for distances of 32, 78, and 100 μm, respectively[37]. Beyond 100 μm, there was no plasma formed in the solution, which may be due to the poor conductivity of pure acetonitrile. Hence, an electrode distance of ~100 μm was maintained for all the experiments. The colorless acetonitrile solution turned pale yellow (240 min) and then dark brown at the end of the reaction (480 min). Radical acetonitrile monomers were initiated at the plasma/acetonitrile interface and underwent further polymerization via a post-plasma-polymerization reaction. To understand the post-plasma-polymerization reaction and the nature of the polymeric compounds at the beginning and end of the reaction, NPs formed by plasma polymerization were characterized using liquid chromatography/mass spectrometry/mass spectrometry (LC/MS/MS) analysis without any dilution. The sample collected at 240 min showed 7 major peaks at m/z (m + 1) 81, 83, 106, 134, 186, 211, and 289, respectively (Fig. 2a). After some time (480 min), the peak intensities of (m + 1) 81, 83, 106, 134, 186, and 211 decreased due to the post-plasma polymerization and intense peaks around (m + 1) 289 formed. Based on LC/MS and MS/MS spectra, the possible structures of 6 polymeric compounds, namely pyrazine, 2,4-dihydro-pyrazine, pyrazine-2-carbonitrile, 2,4a-dihydro-pyrido[2,3-b]pyrazine, 1,4,7,13-pentaaza-anthracene, and 1,4,7,9,13-pentaaza-11-carbonitrile anthracene, are given in Fig. 2. The MS/MS spectra of LM NPs (m + 1: 81, 83, 134, and 186) are identified and the possible structures of the daughter peaks are given in the supplementary section (supplementary Fig. S1). The compound pyrazine-2-carbonitrile follows a fragmented pattern identical to that of 2,4-dihydro-pyrazine. Similarly, 1,4,7,9,13-pentaaza-11-carbonitrile-anthracene follows a pattern identical to that of 1,4,7,13-pentaaza-anthracene (supplementary Table S1).

Optical properties and chemical composition of HM NPs. The ultraviolet-visible (UV-Vis) absorption of NPs gradually increases with increasing contact with plasma. At the end of the reaction, the absorption spectra of NPs shift from UV to the visible region (Fig. 3). As the reaction proceeds, the UV absorption of LM NPs gradually increases from 190 nm (acetonitrile) to 270 nm after a reaction time of 240 min. Beyond 240 min, the brown-colored liquid (HM NPs) showed visible light absorption at 420 nm (Fig. 3 inset). The increase in absorption is due to the post-plasma polymerization of LM NPs, which initiates the formation of nitrogen-enriched ring/

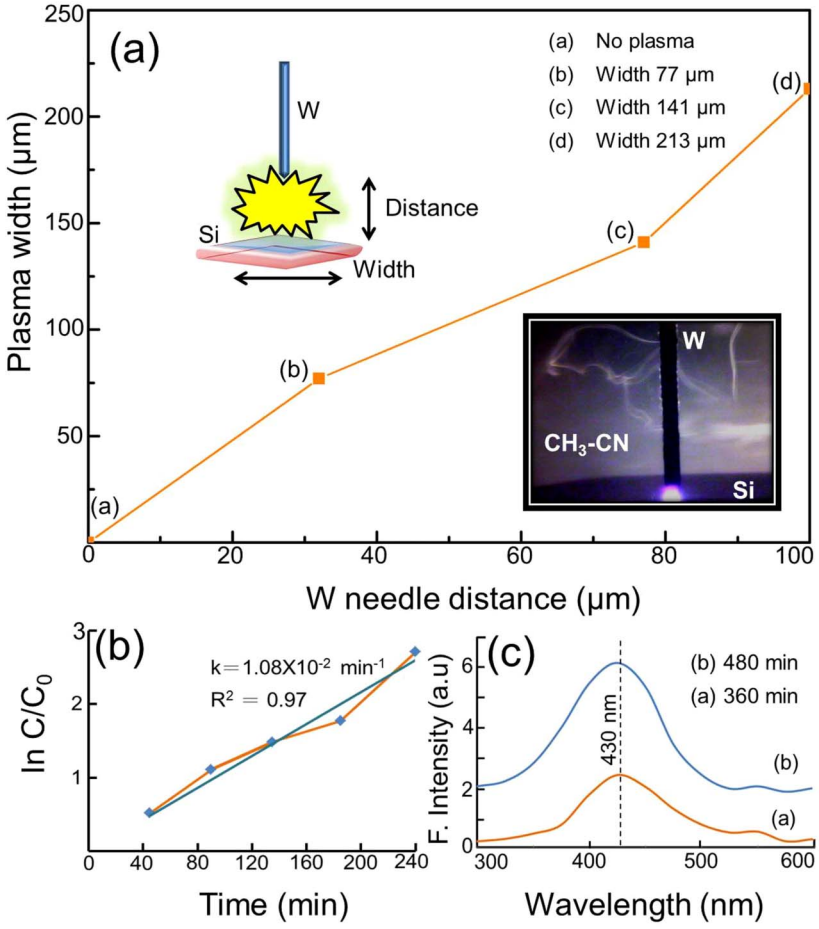

Figure 1 | (a) Correlation diagram for W needle distance versus plasma torch width, (b) reaction rate and order of radical monomers formed in acetonitrile, and (c) fluorescence spectra of NPs collected at 360 and 480 min.

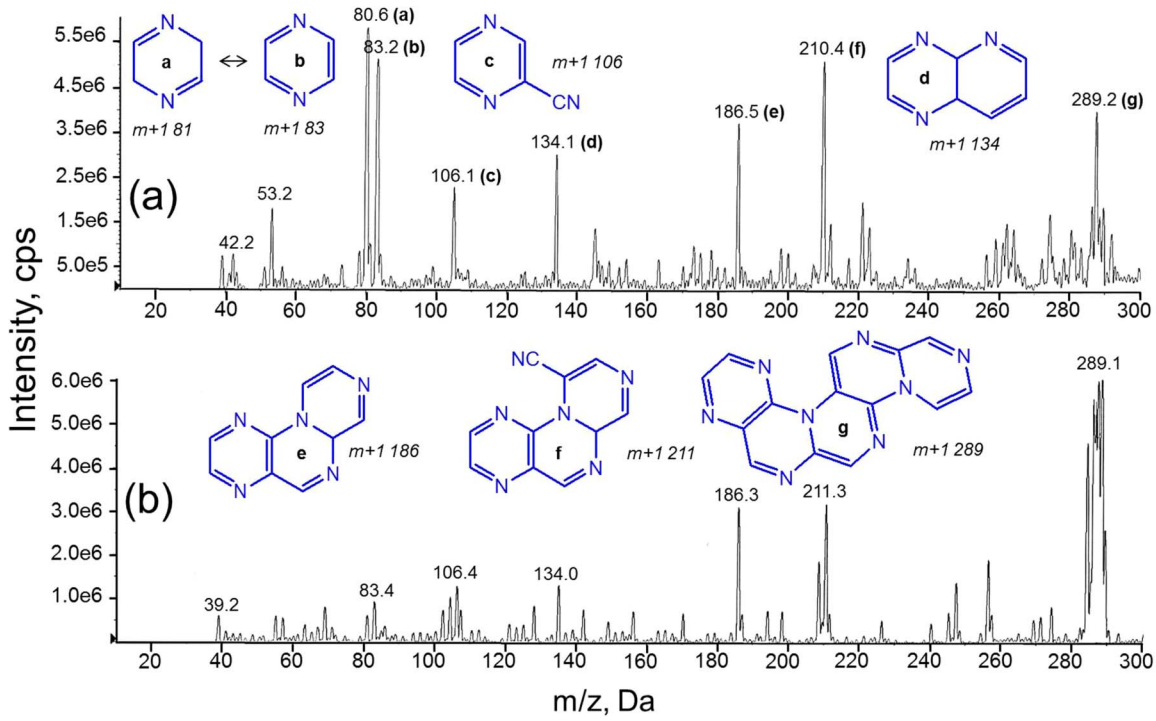

Figure 2 | LC/MS spectra of NPs collected at (a) 240 min and (b) 480 min. Note: (a) 2,4-dihydro-pyrazine, (b) pyrazine, (c) pyrazine-2-carbonitrile, (d) 2,4a-dihydro-pyrido[2,3-b]pyrazine, (e) pyrido[2,3-b]pyrazine, (f) 1,4,7,13-pentaaza-anthracene, and (g) 1,4,7,9,13-pentaaza-11-carbonitrile anthracene.

polymerized structures with external conjugation (C=C, C=N, and C≡N). The formation of LM NPs depends on the reaction rate of ($\cdot CH_2$–C≡N) radical monomer, with other factors, such as plasma intensity, acetonitrile concentration at the interface, and temperature, assumed to be constant. The samples collected at different time intervals showed fluorescence properties when exposed under UV light (254 nm). The fluorescence spectra of NPs collected at 360 min and 480 min are given in the inset of Fig. 1c. The fluorescence spectra show more intense emission at 430 nm for the NPs collected at 480 min when compared to NPs collected at 360 min. The increase in fluorescence may be due to the formation of HM NPs enriched with conjugated nitrogen functional groups. The fluorescence property of the NPs clearly indicates the existence of nitrogen functional groups in the polymerized structures. To determine the rate of formation of the radical monomers at the plasma/acetonitrile interface, the UV absorption (fixed wavelength at 270 nm) value of NPs collected at different time intervals were fitted with pseudo-first-order kinetics. The plot of $\ln[C/C_0]$ vs. t is linear with a correlation coefficient (R^2) value of 0.97 and a rate constant (k) of 1.08×10^{-2} min^{-1} (Fig. 1b). The correlation coefficient (R^2) of 0.97 indicates that the formation of radical monomers at the interface is not affected by the presence of LM NPs and HM NPs in the solution. Hence, the formation of radical monomers in a submerged plasma condition follows pseudo-first-order kinetics and the rate of the formation of LM NPs depends on concentration radical acetonitrile monomers. Scanning electron microscopy (SEM) and high-resolution transmission electron microscopy (HR-TEM) images of concentrated and dried HM NPs are shown in Fig. 4a, Fig. 4b, and Fig. 4c, respectively. The SEM image shows that HM NPs have a uniform surface and a jelly-like appearance. The HR-TEM image shows that HM NPs have a discontinuous amorphous structure with incomplete spheroidal shells. Electron energy loss spectroscopy (EELS) was used to determine the composition of nitrogen and carbon in the NPs. Figure 4d shows the EELS spectrum of HM NPs. It indicates the presence of carbon, nitrogen, and oxygen structures. The sample shows two ionization edges for C-K, at 284 and 287 eV, respectively. Similarly, two ionization edges were observed for N-K, at 399 and 400.4 eV, respectively. This transition of C-K is due to the higher electronegativity of nitrogen atoms, which are present adjacent to the carbon, decreasing the electron density around the carbon atom. Similarly, N-K also shows two ionization edges due to the presence of carbon atoms adjacent to the nitrogen. The peak at 284 eV

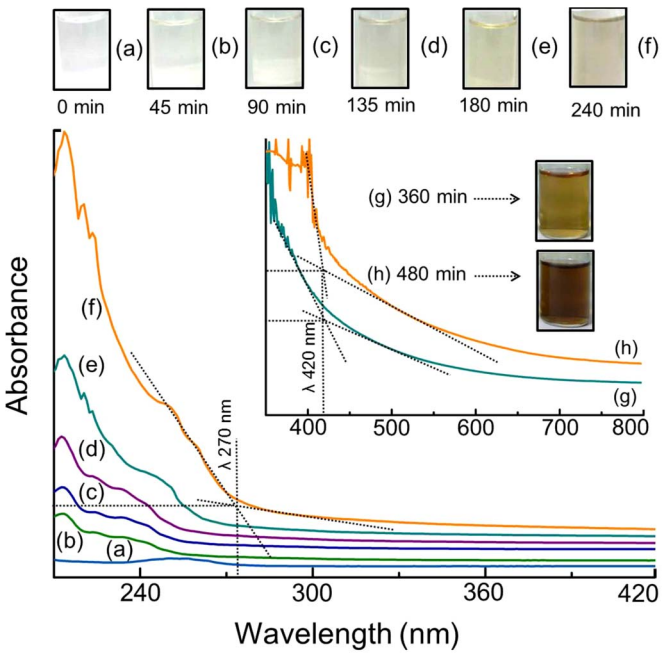

Figure 3 | UV-Vis absorption properties of NPs collected at different time intervals. Inset shows UV-Vis absorption spectra of NPs collected at 360 and 480 min.

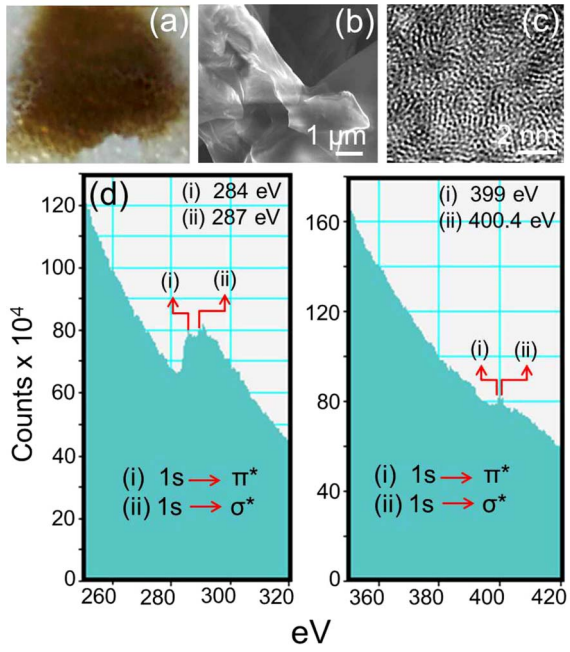

Figure 4 | (a) Image of dried HM NPs. (b) SEM and (c) HRTEM images of HM NPs. (d) EELS spectra of HM NPs. Note: Conditions for EELS spectra for C-K, spectrum acquire 50; exposure 0.5; energy loss 250; dispersion 0.2 eV/ch; aperture 1 mm; and N-K, spectrum acquire 50; exposure 0.5; energy loss 350; dispersion 0.1 eV/ch; aperture 2 mm.

corresponds to the 1s-π* transition, which can be assigned to sp^2 hybridized carbon, and the peak at 287 eV corresponds to the 1s-σ* transition, which can be assigned to sp^2 carbon atoms bonded to nitrogen inside the ring[38]. Similarly, N-K shows two edges, at 399 and 400.4 eV, respectively. The peak at 399 eV is attributed to a pyridine-like structure (imine nitrogen –N), and the peak at 400.4 eV can be assigned to the NC_3 structure in the aromatic ring[38–41]. EELS analysis shows the existence of a pyridine/ring-like structure, which is consistent with the LC/MS/MS analysis. The EELS spectrum with the higher eV was obtained (Supplementary Fig. S2). The O K edge appearing at 536 eV corresponds to the H_2O molecule probably adsorbed from the air.

Structural elucidation of HM NPs. The Raman spectrum of HM NPs shows C–H aromatic stretching vibration modes at 3022 cm^{-1}, 2889 cm^{-1}, and 2851 cm^{-1} and stretching modes of branched C–H at 2740 cm^{-1} (Fig. 5a)[42]. The weak bands at 1658 cm^{-1} and 1601 cm^{-1} are attributed to the C=C stretching vibration mode[42–44]. The band at 1443 cm^{-1} is attributed to the ring semi-circle stretching of a pyridine-like compound[42]. The bands at 1377 cm^{-1} and 1298 cm^{-1} correspond to the presence of polycyclic aromatic compounds and are assigned as the symmetric in-plane ring breathing vibration of the conjugated ring system. The band at 1144 cm^{-1} corresponds to the aromatic ring in breathing mode. The bands at 1092 cm^{-1}, 1088 cm^{-1}, and 986 cm^{-1} are due to the C–H in-plane bending of the heterocyclic/aromatic ring and C–H out-of-plane bending appears at 880 cm^{-1}[42–44]. The Raman spectrum confirms the existence of a pyridine-like structure and shows that carbon is predominantly present in the sp^2 hybridized state. The Fourier transform infrared (FTIR) spectrum of the HM NPs is given in Fig. 5b. The absorption bands in the range of 1100–1650 cm^{-1} correspond to N–C stretching vibrations. Similarly, the

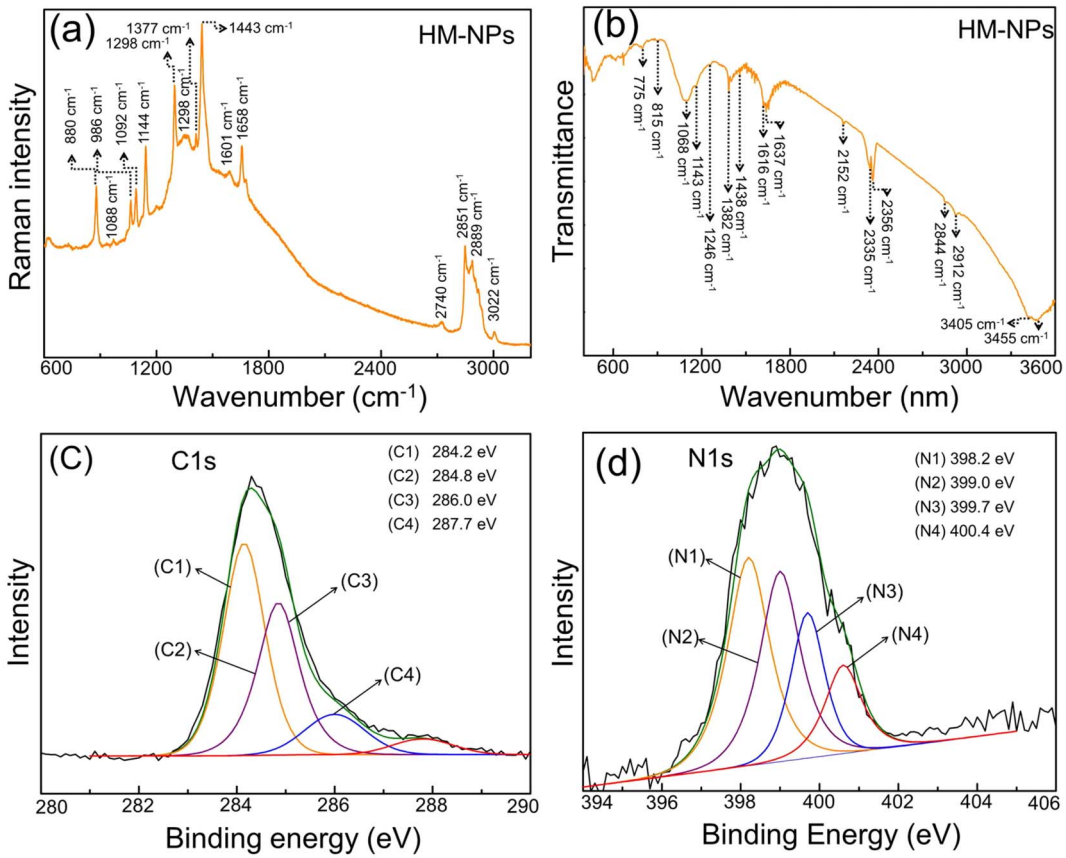

Figure 5 | (a) Raman spectrum and (b) FTIR spectrum of HM NPs. XPS spectra of HM NPs (c) C 1s (d) and N 1s.

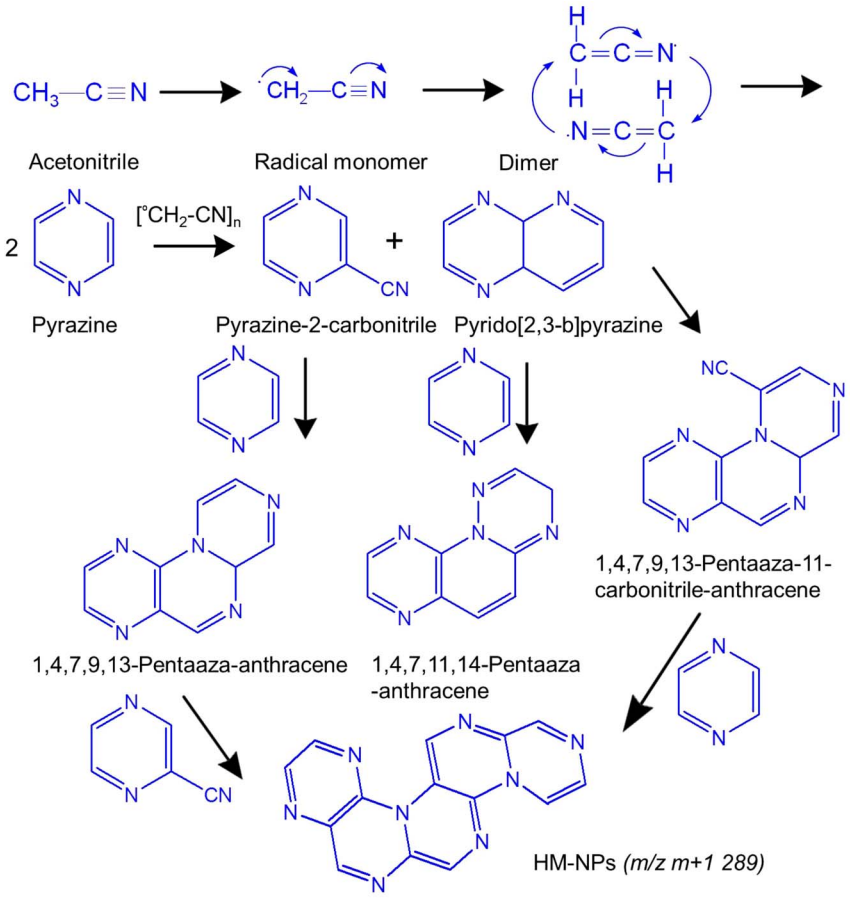

Figure 6 | Proposed reaction mechanism for the formation of LM NPs and HM NPs in submerged liquid plasma.

regions of 1500–1750 cm^{-1} and 2150–2300 cm^{-1} correspond to C=N and C≡N, respectively. The HM NPs show a strong absorption band at 1382 cm^{-1}, which is due to the presence of secondary 2C–N or tertiary 3C–N fragments corresponding to an increase in the C–N single bond character[45,46]. The bands appearing at 1616 cm^{-1} and 1637 cm^{-1} correspond to the stretching vibration mode of C=N. The HM NPs show a very weak band at 2152 cm^{-1}, corresponding to C≡N and confirming the compound (*m/z* 105) mentioned in the LC/MS/MS analysis (Fig. 2a). The N–H stretching vibration mode appears at 2335 cm^{-1}, 3405 cm^{-1}, and 3455 cm^{-1}. The C–H vibration modes appear at 2356 cm^{-1}, 2844 cm^{-1}, and 2912 cm^{-1}.The FTIR and Raman spectra of HM NPs are in good agreement with compounds identified in HM NPs by LC/MS/MS analysis. From elemental analysis, the N/C ratio present in HM NPs was 0.393 (C% 55.53, N% 21.83, and H% 8.91), which is in good agreement with the carbon and nitrogen analyzed in X-ray photoelectron spectroscopy (XPS) analysis. The XPS spectra of HM NPs show peaks for carbon, nitrogen, and oxygen (supplementary Fig. S3). The appearance of an oxygen peak in the XPS spectrum may be due to the hygroscopic nature of HM NPs; oxygen is considered as an impurity. From the XPS analysis, the N/C ratio was found to be 0.362. The electronic 1s core levels of N and C were analyzed and numerically fitted to Gaussian functions (supplementary Table S2). The fittings were similar to the values reported for N 1s and C 1s. The C 1s region consists of four well resolved binding energy configurations identified as 284.2, 284.8, 286.0, and 287.7 eV for C1, C2, C3, and C4, respectively (Fig. 5c). Similarly, N 1s showed binding energy configurations identified as 398.2, 399.0, 399.7, and 400.4 eV for N1, N2, N3, and N4, respectively (Fig. 5d). The broad peak at 398.2 eV can be assigned to the sp^3 C–N bond and that at 400.4 eV can be assigned to sp^2 NC_3 in the aromatic ring[38–41]. The binding energies of 399.0 and 399.7 eV correspond to C=N–C and N–C, respectively. Similarly for C 1s spectra, the binding energies at ~284.2 eV and ~284.8 eV correspond to sp^3 C–C and sp^2 C=C, respectively[6,38,41,47,48]. The binding energies at 286.0 and 287.7 eV are assigned to C_3N in the aromatic ring and C–N, respectively[49,50]. The XPS analysis indicates that the nitrogen is present in the form of C=N–C and can exist only in the form of a ring structure. The binding energies of the above assigned groups are in good agreement with the Raman and FTIR analyses.

Discussion

On the basis of the above experimental results, the possible formation mechanism of unconventional NPs in a submerged plasma condition is proposed. The plasma submerged in acetonitrile initiates hydrogen detachment in the first step, leading to the formation of a highly reactive free-radical monomer ($\cdot CH_2–C\equiv N$) due to the low bond energy of C–H (413 kJ/mol) compared to that of C≡N (891 kJ/mol)[6]. Compounds containing the nitrile group are stable towards electron attack due to the high stability of the C–CN bond and favor plasma polymerization rather than fragmentation[6,28]. The radicalized monomer ($\cdot CH_2–C\equiv N$) is considered as the building block for all 6 compounds and carbon is predominantly present in the sp^2 hybridized form. Nitrogen present in the monomer is sensitive towards radicals, hence electrons from carbon are localized into nitrogen. Carbon is easily attacked by another nucleophile and forms a stable ring structure (Fig. 6). The dimer $C_4N_2H_6$ acts as a base unit for the compounds with a molecular weight of more than 80. The free-radical monomer reacts with the dimer and initiates the formation

of conjugated structure. This structure further undergoes unconventional polymerization by restructuring itself to produce LM NPs. The compounds identified with molecular weights of *m/z* 81 and 83 are considered as dimers of $\cdot CH_2–C\equiv N$. This was further confirmed by their MS/MS daughter peaks, which showed almost identical fragmentation patterns. The LC/MS spectrum shows (Fig. 2b) 5 intense peaks between *m/z* 284 to 290. Due to the existence of a highly reducing environment, LM NPs produce different structures and upon further polymerization form protonated and deprotonated HM NPs between *m/z* 284 to 290. The different protonated structures of HM NPs were not studied further due to the complexity involved in their identification. Hence, the major peak at *m/z* 289 is assigned to the HM NPs and possible reaction mechanisms are considered further. Nitrogen present in the LM NPs shows a high electron withdrawing property, leading to localization of the π bond from the adjacent carbon atom. The electron-deficient carbon is attacked by other nucleophiles (LM NPs) and forms HM NPs. The proposed mechanisms for the formation of LM NPs and HM NPs in a submerged liquid plasma condition are given in Fig. 6. The post-polymerization reaction was initiated only by the nitrile and nitrogen groups in the LM NPs and plasma does not play any role in the formation of HM NPs.

In conclusion, the formation of NPs by the proposed method provides a number of advantages over glow discharge polymerization, including (a) simple reaction set up (b) reaction at ambient conditions, (c) periodic collection of samples allowing clear information about the product, (d) simple procedure, and (e) low operating cost. The formation of NPs in a submerged plasma condition is an eco-friendly single-step process. Further purification is unnecessary and no unwanted by-products are created in this process. Large-scale production could be possible using this method. The NPs are a potential alternative to organic compounds currently used for light harvesting, solar cells, and light-emitting diode applications. The application of a hybrid structure of NPs with nanoparticles is an important challenge for our future research.

Methods

Experiments. In the plasma experiments, an etched tungsten needle was used as a point high-voltage electrode and Si wafer was used as a planar ground electrode. Prior to the experiment, one end of the tungsten needle (<1 mm diameter) was polished using a conventional electrolysis cell[36]. The anodic tungsten needle was inserted into the platinum ring cathode (before etching, ring diameter was 4–5 mm) and 1 M NaOH solution was used as the electrolyte with a cell potential of ~3 V. All the experiments were conducted using a tungsten needle with a diameter of ~75 μm. Acetonitrile (99.95%), procured from Sigma Aldrich, was used as the target material and acetone (Acros, 99.5%) was used as the washing solution. The experiments were conducted in a nitrogen atmosphere to avoid oxygen interference in the acetonitrile polymerization reaction. Both electrodes were immersed into the acetonitrile solution (80 mL) and separated by a distance of ~75 μm. The electrode distance was controlled by a moving stage assembly (Translation Stage Triple-Divide Series 9064 and 9065), which was operated by a computer. A discharge voltage of 2.7 kV was applied (repetition rate: 10 kHz, pulse delay: 500 μs, and pulse width: 5 ms) across the electrodes using a pulse generator (AVTECH, AV-1022-C) connected to a high-voltage amplifier (TREK Model 609E-6), which can generate 0.1 to 5 kV. The plasma polymerization was carried out for a fixed reaction time of 8 h and samples were collected at regular time intervals for further characterization. At the end of the reaction, a clear brown-colored liquid was obtained and no deposition or precipitation was observed on the tungsten needle, grounded electrode, or in the acetonitrile solution. The NP solution was centrifuged to remove trace residual suspended material and the supernatant liquid was used for further analysis.

Characterizations. Absorption spectra of NPs were collected at different time intervals using a UV-Vis spectrometer (SCINCO S-3100). The fluorescence spectra were recorded with a fluorescence spectrophotometer (Hitachi F-4500). The plasma polymerized solution was concentrated by removing unreacted acetonitrile and the residue was used for further characterization. The surface morphology and elemental compositions of the polymerized material were monitored using a high-resolution thermal field-emission scanning electron microscope (FE-SEM, JEOL, JSM-7001). A high-resolution transmission electron microscope (HR-TEM) with an electron energy loss spectroscopy (EELS) analyzer (JEOL JEM 2100F) operating at 200 kV was used to understand the microstructure and surface morphology of the NPs. Raman spectroscopy analysis was performed using a Renishaw inVia confocal micro-Raman spectrometer using a 785-nm argon laser as the excitation source. FTIR spectra of the NPs were recorded using the KBr disk method with Nicolet Nexus 470 and 30 scan were recorded for each sample with a 4 cm^{-1} spectrum resolution. High-resolution X-ray photoelectron spectroscopy (HR-XPS, PHI Quantera SXM, ULVAC Inc., Kanagawa, Japan) was employed to analyze the binding energy of carbon and nitrogen present in NPs. HR-XPS was performed with a monochromatic Al Kα source (25 W, hν = 1486.6 eV) and an energy resolution of 1 eV. All XPS spectra were obtained at a take-off angle of 45° for each element. The atomic sensitivity factors were 0.314, 0.499, and 0.733, corresponding to C 1s, N 1s, and O 1s, respectively. The LC/MS/MS study was carried out using a mass spectrometer (API-4000QTrap) using a turbo ion spray. The electrospray needle was maintained at 5500 V with the declustering potential set at 40 V. Ultrapure nitrogen was used as the nebulizer gas and set at 40 psi. The mass spectrometer was operated in positive ion mode and MS/MS analysis was carried out using nitrogen as the collision gas. The collision energy was kept between 30 and 40 eV. The sample was injected through a syringe pump with a flow rate of 15 μL/min. The elemental composition of NPs was analyzed using an elemental analyzer (Elementar Vario EL III).

1. Boskovic, B. O., Stolojan, V., Khan, R. U. A., Haq, S. & Silva, S. R. P. Large-area synthesis of carbon nanofibres at room temperature. *Nature Mater.* **1**, 165–168 (2002).
2. Chae, S. *et al*. Transferred wrinkled Al_2O_3 for highly stretchable and transparent graphene–carbon nanotube transistors. *Nature Mater.* **12**, 403–409 (2013).
3. Neira-Velazquez, M. G. *et al*. Surface modification of nano clays by plasma polymerization of ethylene plasma process. *Plasma Process Polym.* **8**, 842–849 (2011).
4. Qingsong, Y. U. *et al*. Study of the polymerization mechanism of acetonitrile in glow discharge. *Chinese J. Polym. Sci.* **6(2)**, 172–177 (1998).
5. Herbert, P. A. F., O'Neill, L. & Jaroszynska-Wolinska, J. Soft plasma polymerization of gas state precursors from an atmospheric pressure corona plasma discharge. *Chem. Mater.* **21**, 4401–4407 (2009).
6. Inagaki, N., Tasaka, S. & Yamada, Y. Plasma polymerization of cyano compounds. *J. Polym. Sci. Part A Polym. Chem.* **30(9)**, 2003–2010 (1992).
7. Lefohn, A. E., Mackie, N. M. & Fisher, E. R. Comparison of films deposited from pulsed and continuous wave acetonitrile and acrylonitrile plasmas. *Plasmas and Polym.* **3(4)**, 197–209 (1998).
8. Yoshimura, M. Importance of soft solution processing for advanced inorganic materials. *J. Mater. Res.* **13**(4), 796–802 (1998).
9. Wang, H. & Yoshimura, M. Electrodeposition of diamond like carbon films in organic solvents using thin wire anode. *Chem. Phys. Lett.* **348**, 7–10 (2001).
10. Watanabe, T., Wang, H., Yamakawa, Y. & Yoshimura, M. Direct carbon patterning on a conducting substrate in an organic liquid. *Carbon* **44**, 799–823 (2006).
11. Somiya, S. & Roy, R. Hydrothermal synthesis of fine oxide powders. *Bull. Mater. Sci.* **23(6)**, 453–460 (2000).
12. Lee, M. J. *et al*. A fast, high-endurance and scalable non-volatile memory device made from asymmetric Ta_2O_{5-x}/TaO_{2-x} bilayer structures. *Nature Mater.* **10**, 625–630 (2011).
13. Bhattacharyya, S. *et al*. Localized synthesis of metal nanoparticles using nano-scale corona discharge in aqueous solutions. *Adv. Mater.* **21**, 4039–4044 (2009).
14. Weng, C. C., Hsueh, J. C., Liao, J. D., Chen, C. H. & Yoshimura, M. Rapid micro-scale patterning of alkanethiolate self-assembled monolayers on Au surface by atmospheric micro-plasma stamp. *Plasma Processes Polym.* **10**, 345–352 (2013).
15. Sakiyama, Y., Tomai, T., Miyano, M. & Graves, D. B. Disinfection of E. Coli by non-thermal microplasma electrolysis in normal saline solution. *Appl. Phys. Lett.* **94**, 161501 (2009).
16. Locke, B. R. & Shih, K. Y. Review of the methods to form hydrogen peroxide in electrical discharge plasma with liquid water. *Plasma Sources Sci. Technol.* **20**, 034006 (2011).
17. Weng, C. C. *et al*. Inactivation of bacteria by a mixed argon and oxygen micro-plasma as a function of exposure time. *Int. J. Radiat. Biol.* **85(4)**, 362–368 (2009).
18. Ke, Z., Huang, Q., Zhang, H. & Yu, Z. Reduction and removal of aqueous Cr(VI) by glow discharge plasma at the gas-solution interface. *Environ. Sci. Technol.* **45(18)**, 7841–7847 (2011).
19. Fridman, G. *et al*. Comparison of direct and indirect effects of non-thermal atmospheric-pressure plasma on bacteria. *Plasma Processes Polym.* **4**, 370–375 (2007).
20. Staack, D., Fridman, A., Gutsol, A., Gogotsi, Y. & Friedman, G. Nanoscale corona discharge in liquids, enabling nanosecond optical emission spectroscopy. *Angew. Chem. Int. Ed.* **47**, 8020–8024 (2008).
21. Wang, H. *et al*. Deposition of diamond-like carbon films by electrolysis of methanol solution. *Appl. Phys. Lett.* **69**, 1074–1076 (1996).
22. Toyota, H., Namura, S., Takhashi, Y. & Mukasa, S. Submerged synthesis of diamond in liquid alcohol plasma. *Diam. Relat. Mater.* **17**, 1902–1904 (2008).
23. Chen, Q. *et al*. Microplasma discharge in ethanol solution: Characterization and its application to the synthesis of carbon microstructures. *Thin Films* **516**, 4435–4440 (2008).
24. Liepins, R., Campbell, D. & Walker, C. 1, 2-Dinitrile polymers. I. Hompolymers and copolymers of fumaronitrile, maleonitrile, and succinonitrile. *J. Polym. Sci. A-1* **6**, 3059–3073 (1968).
25. Yasuda, H. & Hirotsu, T. Critical evaluation of conditions of plasma polymerization. *J. Polym. Sci. Polym. Chem. Ed.* **16**, 743–759 (1978).

26. Kobayashi, H., Bell, A. T. & Shen, M. Plasma polymerization of saturated and unsaturated hydrocarbons. *Macromol.* **7(3)**, 277–283 (1974).
27. Yasuda, H. Glow discharge polymerization. *J. Polym. Sci. Macromol. Rev.* **16**, 199–293 (1981).
28. Inagaki, N. *Plasma Surface Modification and Plasma Polymerization* Technomic Publishing Company, Lancaster, PA, (1996).
29. Wang, S., Gaylord, B. S. & Bazan, G. C. Fluorescein provides a resonance gate for FRET from conjugated polymers to DNA intercalated dyes. *J. Am. Chem. Soc.* **126(17)**, 5446–5451 (2004).
30. Tran, H. D., Li, D. & Kaner, R. B. One-dimensional conducting polymer nanostructures: Bulk synthesis and applications. *Adv. Mater.* **21**, 1487–1499 (2009).
31. Patra, A. & Scherf, U. Fluorescent microporous organic polymers: Potential test bed for optical applications. *Chem. Eur. J.* **18**, 10074–10080 (2012).
32. Nyholm, L., Nyström, G., Mihranyan, A. & Strømme, M. Toward flexible polymer and paper-based energy storage devices. *Adv. Mater.* **23**, 3751–3769 (2011).
33. Janoschka, T., Hager, M. D. & Schubert, U. S. Powering up the future: radical polymers for battery applications. *Adv. Mater.* **24**, 6397–6409 (2012).
34. Cheng, C. C. *et al.* Bioinspired hole-conducting polymers for application in organic light-emitting diodes. *J. Mater. Chem.* **22**, 18127–18131 (2012).
35. Chen, J. *et al.* Synthesis and characterization of novel reversible photo-switchable fluorescent polymeric nanoparticles via one-step mini emulsion polymerization. *J. Phys. Chem. B* **115(13)**, 3354–3362 (2011).
36. Kerfriden, S., Nahle, A. H., Campbell, S. A., Walsh, F. C. & Smith, J. R. The electrochemical etching of tungsten STP tips. *Electrochim. Acta* **43**, 1939–1944 (1998).
37. Cheng, H. H., Chen, S. S., Wu, Y. C. & Ho, D. L. Non-thermal plasma technology for degradation of organic compounds in wastewater control: A critical review. *J. Environ. Eng. Manage.* **17(6)**, 427–433 (2007).
38. Mane, G. P. *et al.* Preparation of highly ordered nitrogen - Containing meso porous carbon from a gelatin biomolecule and its excellent sensing of acetic acid. *Adv. Funct. Mater.* **22**, 3596–3604 (2012).
39. Johanson, A. & Stafstrom, S. A self-consistent-field study of the nitrogen 1s binding energies in carbon nitrides. *J. Chem. Phys.* **111**, 3203–3208 (1999).
40. Hammer, P. & Alvarez, F. Influence of chemical sputtering on the composition and bonding structure of carbon nitride films. *Thin Solid Films* **398–399**, 116–123 (2001)
41. Cho, Y. J. *et al.* Selective nitrogen-doping structure of nano size graphitic layers. *J. Phys. Chem. C* **115**, 3737–3744 (2011).
42. Larkin, J. *Infrared and Raman Spectroscopy: Principles and Spectral Interpretation.* Elsevier Publication, (2011).
43. Dollish, F. R., Fateley, W. G. & Bentley, F. F. *Characteristic Raman Frequencies of Organic Compounds.* John Wiley, New York, (1974).
44. Li, W. H., Li, X. Y. & Yu, N. T. Surface-enhanced hyper-Raman spectroscopy SEHRS/and studies of pyrazine and pyridine adsorbed on silver electrodes. *Chem. Phys. Lett.* **305(3–4)**, 303–310 (1999).
45. Miller, D. R., Wang, J. & Gillan, E. G. Rapid, facile synthesis of nitrogen-rich carbon nitride powders. *J. Mater. Chem.* **12**, 2463–2469 (2002).
46. Zhao, Y. *et al.* Large-scale synthesis of nitrogen-rich carbon nitride microfibers by using graphitic carbon nitride as precursor. *Adv. Mater.* **20(9)**, 1777–1781 (2008).
47. Presser, V., Heon, M. & Gogotsi, Y. Carbide-derived carbons from porous networks to nanotubes and graphene. *Adv. Funct. Mater.* **21**, 810–833 (2011).
48. Sawa, K. G. & du-Plessis, J. The X-ray photoelectron spectroscopy C 1s diamond peak of chemical vapor deposition diamond from a sharp interfacial structure. *Mater. Lett.* **58**, 1344–1348 (2004).
49. Marton, D., Boyd, K. J. & Rabalais, J. W. Synthesis of carbon nitride. *Int. J. Mod. Phys. B* **9(27)**, 3527–3558 (1995).
50. Sun, L. *et al.* Nitrogen-doped graphene with high nitrogen level via a one-step hydrothermal reaction of graphene oxide with urea for superior capacitive energy storage. *RSC. Adv.* **2**, 4498–4506 (2012).

Acknowledgements

The authors are grateful to Prof. Yury Gogotsi, Department of Materials Science and Engineering, and A. J. Drexel Nanotechnology Institute, Drexel University, Philadelphia, PA 19104, USA for providing fruitful discussion and support.

Author contributions

M.Y. and J.S.N. performed the experimental planning, experimental measurements, data examination, and manuscript preparation. J.D.L. contributed to the experimental setup, planning, and data analysis. C.C.W. contributed to the experimental setup and optimized plasma discharge in a submerged condition.

Additional information

Supplementary information accompanies this paper at http://www.nature.com/scientificreports

Competing financial interests: The authors declare no competing financial interests.

How to cite this article: Senthilnathan, J., Weng, C.-C., Liao, J.-D. & Yoshimura, M. Submerged Liquid Plasma for the Synthesis of Unconventional Nitrogen Polymers. *Sci. Rep.* **3**, 2414; DOI:10.1038/srep02414 (2013).